

# Quantitative intravital microscopy of hepatic transport

Clifford M. Babbey,<sup>1,†</sup> Jennifer C. Ryan,<sup>1</sup> Erin M. Gill,<sup>2,‡</sup> Marwan S. Ghabril,<sup>3</sup> Courtney R. Burch,<sup>4</sup> April Paulman<sup>4</sup> and Kenneth W. Dunn<sup>1,\*</sup>

<sup>1</sup>Department of Medicine; Division of Nephrology; Indiana University Medical Center; Indianapolis, IN USA; <sup>2</sup>INphoton, LLC; Indianapolis, IN USA;

<sup>3</sup>Department of Medicine; Division of Gastroenterology/Hepatology; Indiana University Medical Center; Indianapolis, IN USA; <sup>4</sup>Covance Laboratories; Greenfield, IN USA

Current affiliations: <sup>†</sup>Wells Center for Pediatric Research; Indiana University Medical Center; Indianapolis, IN USA; <sup>‡</sup>WiSys Technology Foundation, Inc.; Madison, WI USA

**Keywords:** intravital microscopy, hepatocyte, liver, transport, hepatotoxicity, cholestasis

Intravital microscopy has a long history of application to studies of the liver. Here we demonstrate how intravital multiphoton microscopy may be combined with digital image analysis to quantitatively evaluate the effects of drugs on hepatocyte transport in vivo.

## Introduction

The liver performs a number of critical physiological functions. In addition to producing a variety of important proteins and cholesterol, the liver is responsible for processing nutrients, producing bile and removing toxins from the blood. It is this last function that is particularly significant medically, because the liver provides one of the major avenues of drug metabolism and excretion. Accordingly, a major component of pharmacology in drug development involves understanding how the liver transports candidate compounds. However, it is frequently equally important to understand how candidate compounds impact liver transport, effects that may manifest themselves in drug-drug interactions or in liver injury. Indeed, drug-induced liver injury is the single biggest source of failure of drugs in development<sup>1</sup> and the primary reason for withdrawal of approved drugs from the market.<sup>2</sup>

The fundamental process of liver transport is one in which compounds present in the blood are transported into hepatocytes, where they may be metabolized and secreted into the bile. While simple in concept, the process is actually quite complex. First, the liver transports a diverse array of substrates via a large number of different transporters with overlapping specificities, making it difficult to attribute transport to a particular transporter pathway or to predict drug-drug interactions. Second, vectorial transport depends upon the abundance and polarized expression of specific transporters to either the sinusoidal (blood) or canalicular (bile) membranes, both of which are acutely regulated in timescales varying from minutes<sup>3,4</sup> to days.<sup>5-7</sup> Finally, while hepatic transport is generally schematized in terms of a single hepatocyte, the process is actually mediated at the functional level of the lobule; blood flowing from the periportal to pericentral veins

sequentially encounters hepatocytes with varying expression of different transporters, each regulated differently in response to cholestatic injury.<sup>8-10</sup>

Because of this complexity, it is frequently difficult to predict the in vivo effects of drugs from those observed in cultured cell systems. On the other hand, it is nearly impossible to identify the underlying mechanism of transport effects from the composite readouts provided by traditional animal pharmacology and toxicology studies. As described below, we have developed methods of quantitative intravital microscopy that support analysis of hepatic transport in vivo at the level of individual hepatocytes, providing a powerful tool for understanding complex effects on hepatic transport.

## Results

The liver is well-suited to the specific requirements of intravital microscopy. The liver can be easily exposed and imaged with minimal surgical preparation and manipulation. The liver is a homogeneous organ, in that processes of drug transport, drug distribution and cellular function can be characterized by sampling cells located within the working distance of the microscope objective, without the need to surgically expose deeper regions of the liver. Various aspects of liver function can be investigated using probes that are simply introduced via intravenous injection. Accordingly, intravital microscopy has been applied to a wide range of studies of the liver. Intravital microscopy has been almost routinely used to characterize microvascular flow in the liver,<sup>11-13</sup> but has also been used to assay hepatocyte cell death<sup>14-20</sup> apoptosis,<sup>21</sup> inflammatory cell infiltration,<sup>22-24</sup> microvascular permeability,<sup>25-27</sup> mitochondrial function,<sup>14,15,17-19,28,29</sup> steatosis,<sup>30,31</sup> tumor angiogenesis<sup>32</sup> and fibrosis.<sup>33</sup> Fluorescent transport substrates

\*Correspondence to: Kenneth W. Dunn; Email: kwdunn@iupui.edu  
Submitted: 06/01/12; Revised: 06/27/12; Accepted: 06/28/12  
<http://dx.doi.org/>

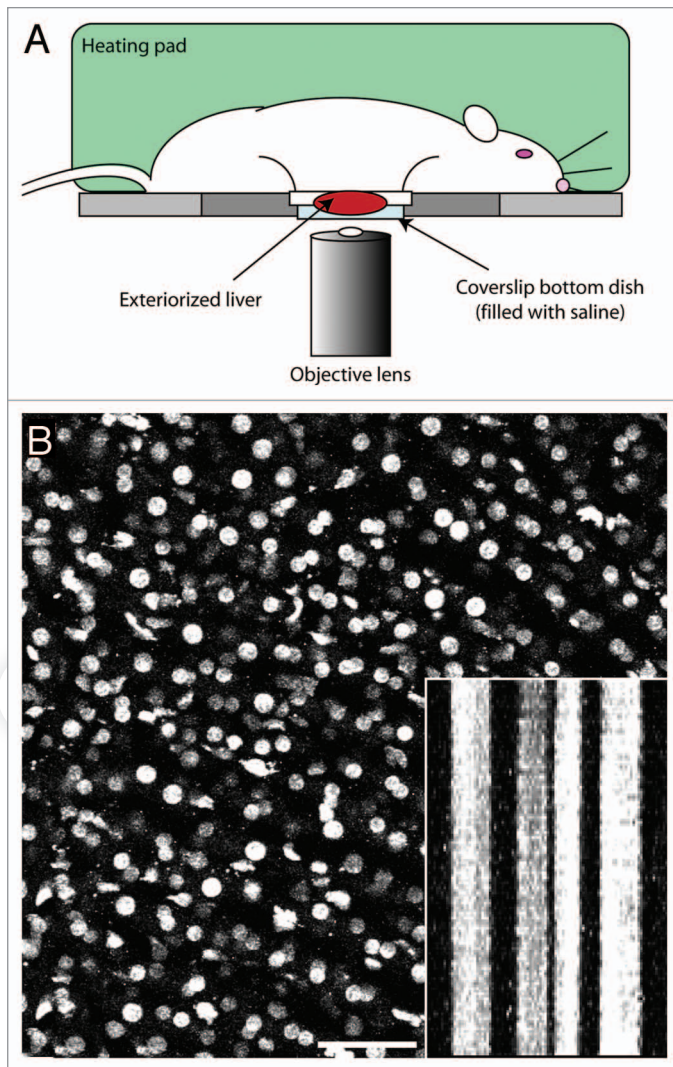


**Figure 1.** Immobilization of the rat liver for intravital microscopy. (A) Schematic diagram of how the liver is presented to the microscope objective for microscopy. (B) Maximum projection of an image volume, consisting of 6 images collected 1 micron apart, from the liver of a living rat after intravenous injection of Hoechst 33342, which labels cell nuclei. This image is the maximum projection of the first of 75 sequential volumes collected over a period of 12 min. The time series of projected images is shown in Video S1. Inset - an XT image of the time series of image projections. This image shows the intensity along a 3 pixel wide line profile through 4 adjacent nuclei (horizontal axis) over the 12 min interval (vertical axis). Scale bar represents a distance of 50 microns.

have also been used in combination with intravital microscopy to characterize hepatic transport *in vivo*.<sup>34-42</sup> As outlined below, we have adapted and extended the approaches used in these studies into quantitative assays of hepatocyte transport.

**Immobilization of the liver for high resolution microscopy.** The transport assays described below are based upon measurement of the changes in fluorescence in subcellular compartments over time after intravenous injection of fluorescent transport substrates. Quantifying changes in fluorescence in structures as narrow as the bile canaliculus requires extraordinary specimen stability. While this kind of stability is easily achieved in cultured

cell systems, it is more difficult to achieve in intravital microscopy, especially in the liver, whose proximity to the diaphragm makes it particularly susceptible to respiration-induced motion.

We have combined two approaches that together minimize motion artifacts in intravital microscopy of the rat liver. First, we have developed a procedure in which the surgically exposed liver is essentially tethered to a coverslip-bottomed dish with gauze (as fully described in the Methods section). As shown in **Figure 1A**, the liver of the living rat is then imaged from below via an inverted microscope. Using multiphoton fluorescence microscopy, this arrangement provides access to depths up to 100 microns into the rat liver. Second, to minimize the effects of residual vertical tissue motion (along the optical axis), we collect 3D image volumes (5–6 focal planes, spaced 1 micron apart) at each time point. By converting each of these volumes into a single maximum projection image, images of structures located within the image volumes will be consistently collected throughout the entire time series, regardless of small vertical translations in the tissue, and the quantitative effects of vertical motion minimized.

The effectiveness of these approaches is demonstrated in an experiment in which we collected a time series of image volumes from the liver of a rat that had received an intravenous injection of Hoechst 33342, a DNA-binding fluorophore that labels nuclei *in vivo*.<sup>43</sup> Over the course of 12 min, 75 image volumes were collected. Each volume was converted into a single maximum projection, and the series of maximum projections was assembled into a time series. Presented in **Video S1**, this time series shows impressive stability with imperceptible lateral motion in hepatocyte nuclei. Readers may also notice migratory cells, likely to be NKT cells, patrolling the sinusoids. **Figure 1B** shows the first image in this time series, and the inset shows an intensity profile of a 3 pixel wide line through 4 nuclei (on the horizontal axis) collected over the entire 75 image time series (arrayed along the vertical axis). This image demonstrates that the sample has been immobilized to single pixel lateral stability (0.6 microns).

**Quantitative microscopic analysis of sodium fluorescein transport in the rat liver.** Sodium fluorescein (also known as uranine) is the sodium salt of fluorescein, a fluorescent anion. In one of its first applications in 1877, fluorescein was used to demonstrate that the Danube sinkhole, into which the Danube river disappears several times a year, is the source of water emerging from the Aatchopf spring, some 12 km away. Still used in environmental studies, sodium fluorescein is widely used clinically, particularly for retinal angiography, a procedure in which fluorescence imaging is used to evaluate retinal perfusion. With minimal toxicity (LD<sub>50</sub> of 1 g/kg in rats), sodium fluorescein has been frequently used as a fluorescent probe in intravital microscopy studies of hepatic transport,<sup>34,35,39,40,44,45</sup> although it has only recently been demonstrated to be a specific substrate of the human and rat organic anion (OAT/Oat) transporters.<sup>46</sup> Like many other substrates transported by hepatocytes, fluorescein is rapidly glucuronidated in the cytosol following hepatocyte uptake,<sup>47-49</sup> making it an appropriate model probe for the anion glucuronate transporters Mrp2 and Mrp3.

**Figure 2** shows a schematic diagram of hepatic transport of fluorescein following intravenous injection. First, limited to the

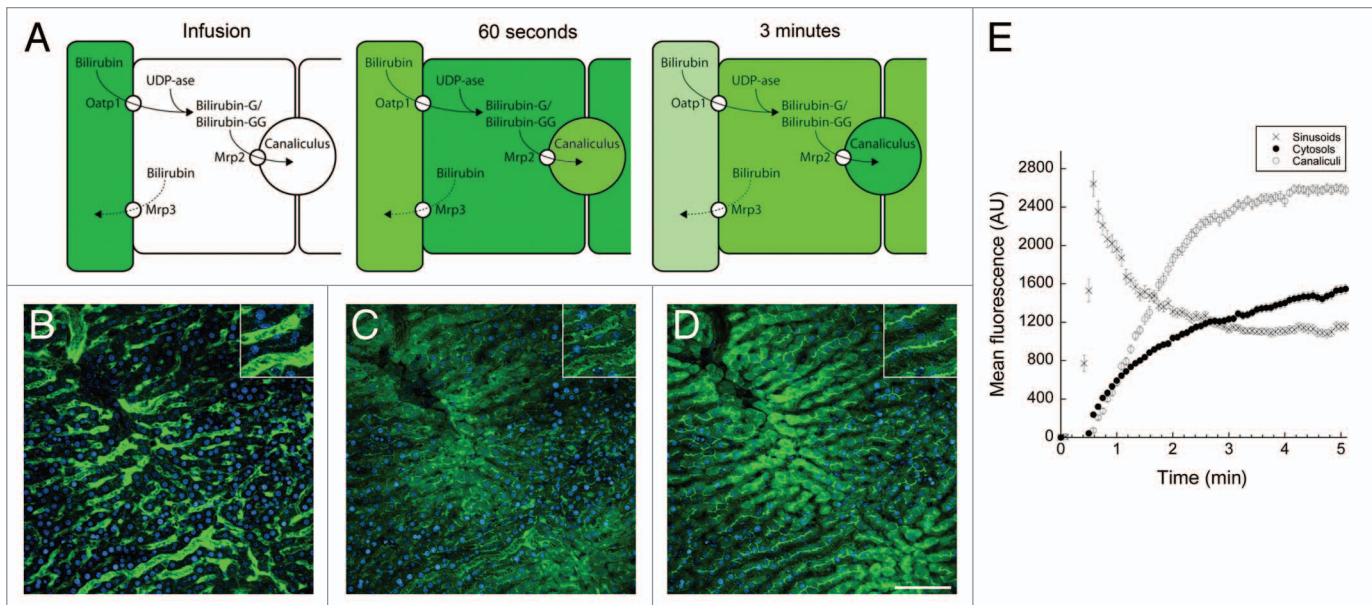


**Figure 2.** Time course of sodium fluorescein transport in the rat liver. (A) Schematic diagram of the sequential appearance of an intravenously-introduced bolus of sodium fluorescein first in the sinusoid (left panel), then in the hepatocyte cytosol (middle panel) and finally in the bile canaliculus (right panel). (B–D) Maximum projections of image volumes collected in the liver of a living rat at the time of infusion of a bolus injection of sodium fluorescein (B), 60 sec after infusion (C) and 3 min after infusion (D). Sodium fluorescein appears first in the vasculature immediately after injection, subsequently redistributing to the hepatocyte cytosol and ultimately to the bile canaliculi. Nuclei are labeled with Hoechst 33342, introduced prior to injection of sodium fluorescein. The entire time series of 122 maximum projections collected over ten minutes is shown in Video S2. Scale bar represents a distance of 100 microns. Inserts at top right of each panel show 2X magnifications of a region at the mid-bottom of the field. (E) Quantification of the mean fluorescence of 44 regions in the hepatocyte cytosol (closed circles), adjacent canaliculi (open circles) and adjacent sinusoid (crosses) over a period of 5 min. Probe injection was conducted at approximately 30 sec.

sinusoids (left compartment in left panel), fluorescein is rapidly internalized into hepatocytes by organic anion transporters (middle panel), and subsequently secreted into bile canaliculi (right panel). **Figures 2B–D** show corresponding projection image volumes collected from the liver of a living rat following intravenous injection of a bolus (2.5 mg/kg) of sodium fluorescein. Careful comparison of these images shows that, fluorescein is limited to the sinusoids at infusion, beginning to appear in hepatocytes by 60 sec and finally brightly accumulating in canaliculi within 3 min of infusion. The kinetics of this redistribution are clearer in **Video S2**, which shows a time series of 122 projected image volumes collected over 10 min. Essentially identical results to those presented in **Figure 2** have been obtained in 5 additional rats.

In order to quantify hepatic transport, we identified 44 hepatocytes in the field shown in **Figure 2**, and for each, demarcated a 10 pixel region of interest in the canaliculus, surrounding cytosol and adjacent sinusoid. For each cell, we quantified the mean fluorescence in each of these regions for each time point, correcting for background by subtracting the mean value measured just prior to infusion. The results of this analysis are presented in **Figure 2E**. The rate of hepatocyte uptake can be quantified as the initial rate of linear increase in mean fluorescence in the hepatocyte cytosol (mean of 1391 AU (Arbitrary Units of fluorescence) per minute) and the rate of canalicular secretion as the initial rate of linear increase in mean fluorescence in the canaliculus (mean of 1263 AU per minute).

**Effect of rifampin on sodium fluorescein transport in the rat liver.** In order to demonstrate the sensitivity of the liver transport assays, we evaluated transport in rats treated for 4 d with rifampin, an antibiotic used to treat tuberculosis, and a potent inhibitor of rat and human organic anion transporters.<sup>50–54</sup> The time course of fluorescein redistribution over 6 min in rifampin-treated and vehicle-treated control rats is shown in **Figure 3**. The top three panels show that, similar to the results shown in **Figure 2**, fluorescein rapidly redistributes from the sinusoids into the hepatocyte cytosol and canaliculi in a control rat. In contrast, over this same time interval fluorescein appears to remain restricted to sinusoids in rifampin-treated rats. The difference in transport between the two rats is clearly demonstrated in **Video S3**, which shows a time series of 40 projected image volumes of these two fields collected over 6 min. These observations are supported with quantitative analyses, summarized in **Figure 3G and H**. As in **Figure 2E**, quantitative analysis of the vehicle-treated control rat demonstrates rapid hepatocyte uptake and canalicular secretion. In contrast, the rifampin-treated rat was characterized by a protracted retention of fluorescein in the sinusoids, minimal cytosolic uptake and undetectable canalicular secretion.

Although we are interested in measuring changes in the concentration of fluorescent probes in different compartments over time, we actually measure changes in detected fluorescence, which is a function not only of probe concentration, but also the efficiency with which fluorescence is stimulated, collected and converted into a digital signal. Thus, if measurements from

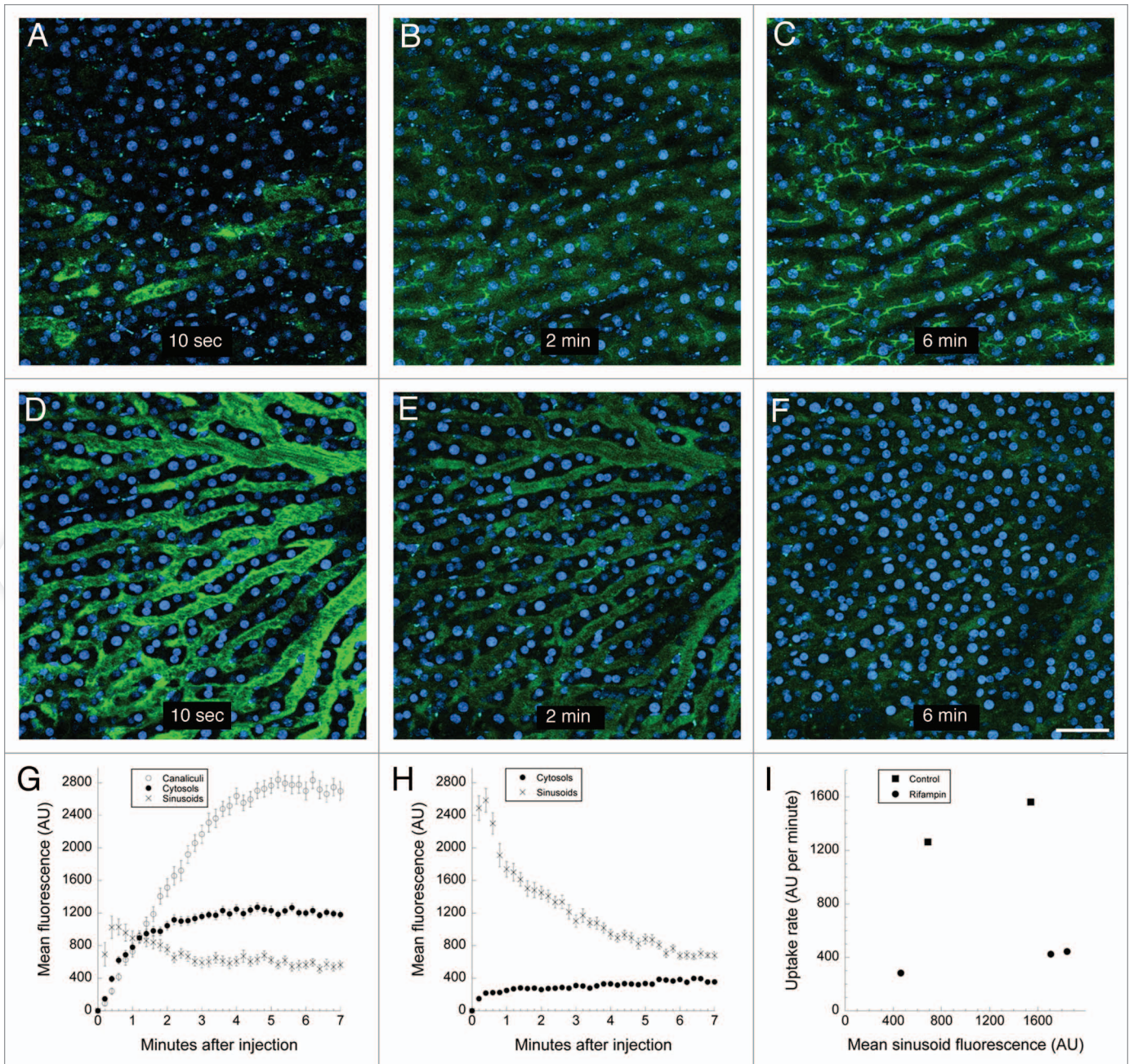


**Figure 3.** Effects of rifampin on transport of sodium fluorescein in the rat liver. A - C - Maximum projections of image volumes collected in the liver of a living rat 10 sec (A), 2 min (B) and 6 min (C) after injection of sodium fluorescein. (D-F) corresponding images collected from the liver of a rat treated for 4 d with 250 mg/kg rifampin by oral gavage. Nuclei are labeled with Hoechst 33342, introduced prior to injection of sodium fluorescein. Whereas in the vehicle-treated rat, sodium fluorescein rapidly redistributed from the sinusoids to the hepatocyte cytosol to the bile canaliculi, sodium fluorescein is largely retained in the sinusoids in the rat treated with rifampin. Scale bar represents a distance of 50 microns. The time series of 40 maximum projections collected over 6 min for both the control and rifampin-treated rats is shown in Video S3. (G) Quantification of the mean fluorescence of 28 regions in the hepatocyte cytosol (closed circles), adjacent canaliculi (open circles) and adjacent sinusoid (crosses) collected from the vehicle-treated rat over a period of 7 min after bolus injection of sodium fluorescein. (H) Quantification of the mean fluorescence of 26 regions in the hepatocyte cytosol (closed circles), adjacent canaliculi (open circles) and adjacent sinusoid (crosses) collected from the rat treated with rifampin over a period of 7 min after bolus injection of sodium fluorescein. (I) Plots of cytosolic uptake rates as a function of mean sinusoid fluorescence (quantified during the first 30 sec) for three rats treated with rifampin (circles) and 2 rats treated with vehicle alone (squares).

different studies are to be pooled for comparison, they must be collected from the same depth in the liver, identical laser illumination levels, an identical excitation wavelength and pulse duration, the same objective lens and identical photomultiplier

detection settings. **Figure 3I** shows the results of quantitative analysis of fluorescence microscopic studies of 3 rifampin and 2 vehicle-treated rats, all conducted with identical microscope settings. Since we anticipate that hepatocyte uptake of sodium

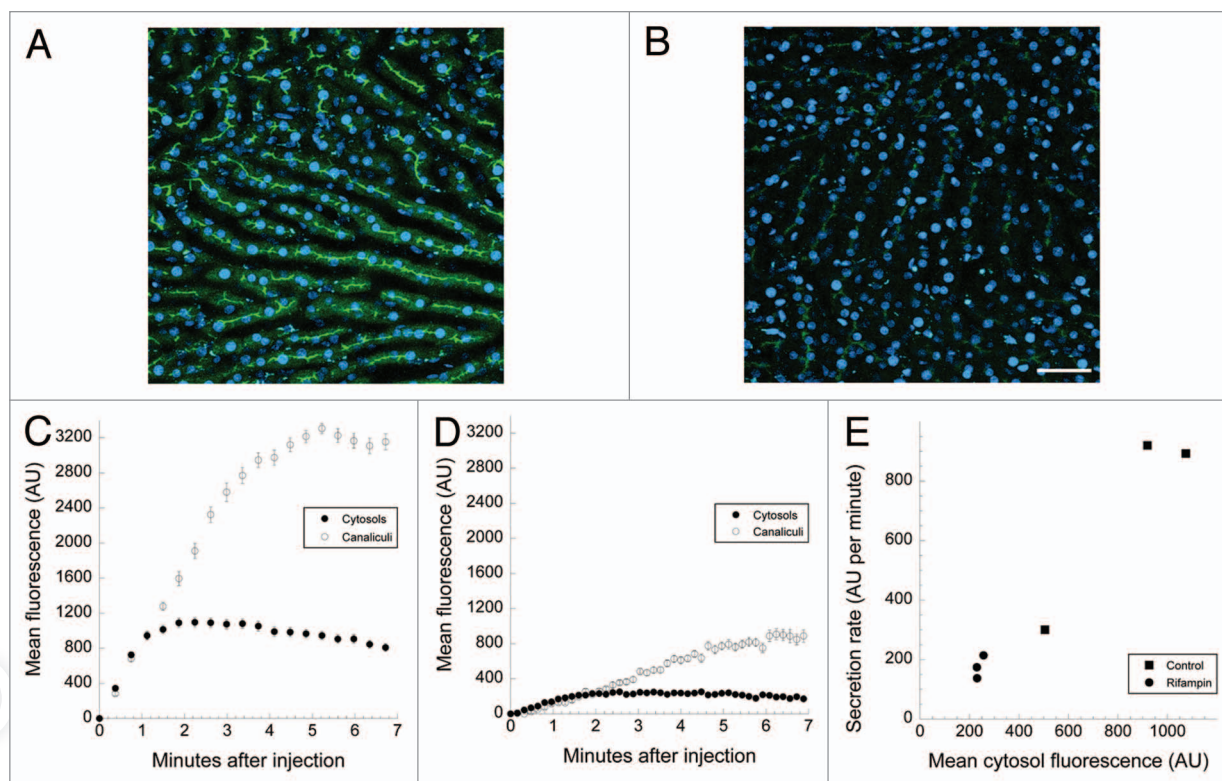


**Figure 4.** Effect of rifampin on secretion of 6-carboxy fluorescein in the rat liver. (A) Maximum projection of an image volume collected from the liver of a living rat 6 min after injection of 6-CFDA. (B) Corresponding projection image collected from the liver of a rat treated for 4 d with rifampin. Nuclei are labeled with Hoechst 33342, introduced prior to injection of sodium fluorescein. Whereas in the vehicle-treated rat, 6-CF fluorescence rapidly accumulates to high levels in the bile canaliculi, 6-CF accumulates more slowly and to a lower level in canaliculi of the rat treated with rifampin. Scale bar represents a distance of 50 microns. The time series of maximum projections collected over 12 min for both the control and rifampin-treated rats is shown in Video S4. (C) Quantification of the mean fluorescence of 36 regions in the hepatocyte cytosol (closed circles) and adjacent canaliculi (open circles) collected from the vehicle-treated rat over a period of 7 min after bolus injection of 6-CFDA. (D) Quantification of the mean fluorescence of 27 regions in the hepatocyte cytosol (closed circles) and adjacent canaliculi (open circles) collected from the rat treated with rifampin over a period of 7 min after bolus injection of 6-CFDA. (E) Plots of the rates of canalicular secretion as a function of mean cytosolic fluorescence (quantified from 1.5 to 3 min after injection) for three rats treated with rifampin (circles) and 3 rats treated with vehicle alone (squares).

fluorescein will follow a Michaelis-Menton function of concentration in the sinusoid, we have plotted the initial rate of probe uptake (the rate of increase in mean cytosolic fluorescence over the first 30 sec after probe injection) as a function of measured concentration in the sinusoids (the mean fluorescence in the adjacent sinusoid space over this same time interval). This plot clearly demonstrates that rifampin significantly reduces the rate of hepatocyte uptake over a range of different sinusoid concentrations. If data are pooled for each condition, rifampin decreased the mean rate of uptake from 1412 to 434 AU per minute, a reduction of nearly 70%. These results demonstrate that, consistent with previous studies of cultured cells, rifampin inhibits hepatocyte organic anion uptake *in vivo*.

#### Effect of rifampin on hepatocyte secretion in the rat liver.

Previous studies of cultured rat hepatocytes indicate that rifampin also inhibits Mrp2-mediated canalicular secretion.<sup>55,56</sup> Assaying the effect of rifampin on hepatocyte secretion using sodium fluorescein as a probe is confounded by the fact that rifampin significantly blocks hepatocyte uptake of sodium fluorescein (Fig. 3). In order to circumvent this problem, we evaluated the effects of rifampin on canalicular secretion in a second set of studies in

which transport was quantified using 6-carboxyfluorescein diacetate (6-CFDA) as a probe. Unlike sodium fluorescein, 6-CFDA is membrane permeant and essentially non-fluorescent. However, upon exposure to esterases (for example in the hepatocyte cytosol), 6-CFDA is cleaved to form 6-carboxyfluorescein (6-CF), a molecule that is both highly fluorescent and charged. The charge renders the molecule membrane impermeant, so that its secretion can be used to assay efflux transporter activity. Previous studies have verified that its efflux is mediated by Mrp2 and Mrp3<sup>57</sup> and 6-CFDA has been used to quantify hepatocyte transport *in vitro*<sup>56</sup> and *in vivo*.<sup>37,38</sup>

The results of studies using 6-CFDA to assay the effect of rifampin on canalicular secretion are summarized in Figure 4. Figure 4A shows an example of a projected image volume collected from the liver of a vehicle-treated living rat, 6 min after intravenous injection of 6-CFDA. The accumulation of 6-CF in the cytosol and especially the canaliculi in the control rat contrast with the much dimmer fluorescence found in hepatocytes in the liver of a rat treated with rifampin (Fig. 4B). The difference in transport between the two rats is clearly demonstrated in Video S4, which shows the time series of projected image

volumes for both control and rifampin-treated rats collected over 12 min after 6-CFDA injection. Whereas in the control, 6-CF fluorescence rapidly appears and accumulates in the hepatocyte cytosol and canaliculi (without appearing in the sinusoids), 6-CF fluorescence slowly accumulates to modest levels in the canaliculi of the rifampin-treated rat.

These qualitative observations are supported by the quantitative analyses of the kinetics of 6-CF fluorescence in the cytosol and canaliculi of control and rifampin-treated rats, examples of which are shown in **Figure 4C and D**, respectively. While these curves demonstrate that rifampin profoundly slowed net canalicular secretion of 6-CF, the effect of rifampin on Mrp2 activity is less clear when one factors in differences in the cytosolic concentration of 6-CF. **Figure 4E** shows the results of studies of 3 control and 3 rifampin-treated rats, in which the initial rates of canalicular secretion (measured as the mean rate of fluorescence increase in the canaliculi over the interval between 1.5 and 3 min after probe injection) are plotted as a function of mean cytosolic fluorescence (during the same interval). The essentially linear relationship between the rate of canalicular secretion and mean cytosolic fluorescence in the combined data indicates that transport of 6-CF into canaliculi is substrate-limited in the range of cytosolic concentrations of 6-CF obtained in these studies. While the rates of canalicular secretion of rats treated with rifampin are lower than those for vehicle-treated rats, they fall on the same linear relationship between secretion rate and cytosolic fluorescence found for vehicle-treated rats, consistent with the idea that the slowed secretion observed in rifampin-treated rats results simply from reduced amount of cytosolic 6-CF. Consistent with this interpretation, the 4-fold decrease in transport rate agrees well with the 3.5 fold decrease in cytosolic concentration. Thus, while these data demonstrate that rifampin clearly decreases transport to canaliculi, they do not indicate an effect on Mrp2 activity.

## Discussion

The studies presented here demonstrate how the spatial and temporal resolution provided by intravital multiphoton microscopy can be combined with digital image analysis into a quantitative tool for understanding complex drug effects on hepatic transport *in vivo*. Intravital microscopy provides the capability to dissect hepatic transport in ways traditionally associated with studies of cultured cells, but in the relevant context of the intact animal model.

In particular, studies of rats demonstrated that repeated administration of rifampin causes a significant reduction of hepatocyte uptake of sodium fluorescein *in vivo*. This result is consistent with previous studies in which rifampin has been found to inhibit hepatic uptake in cultured rat hepatocytes<sup>51</sup> and perfused rat liver.<sup>53</sup> However, our results are novel in that they, (1) demonstrate that rifampin blocks uptake by hepatocytes in the intact liver *in vivo*, (2) demonstrate that rifampin blocks the initial step of uptake into the cytosol and (3) demonstrate that inhibition occurs with chronic administration of rifampin. Based upon previous studies demonstrating that rifampin inhibits transport in cell systems expressing human and rat organic

anion transporters,<sup>50,52,53</sup> we interpret our results to indicate that chronic treatment with rifampin results in inhibition of organic anion transporters in the liver of rats.

While we observe a net decrease in canalicular secretion in rifampin-treated rats, the decrease was proportional to the decreased amount of fluorescent probe delivered into the cytosol, and thus most easily explained by an effect on uptake. This result contrasts with previous fluorescence microscopy studies indicating that rifampin reduces canalicular secretion of dichlorofluorescein in cultured hepatocytes<sup>55,56</sup> and studies of transfected cell systems indicating that rifampin blocks human and rat MRP2-mediated transport.<sup>53,55,56,58</sup> The basis of this difference is unclear, but may reflect differences between the *in vitro* and *in vivo* context of the different studies.

It is unclear why so little 6-CF was observed in the hepatocyte cytosol and canaliculi of rats treated with rifampin. In this regard, the studies of Zamek-Gliszczynski and colleagues<sup>57</sup> may be informative. These studies found that 6-CFDA is rapidly hydrolyzed to 6-CF when incubated with 20% rat blood. Thus, in contrast to assumptions that 6-CF accesses the hepatocyte cytosol *in vivo* via its membrane-permeant parent compound 6-CFDA, 6-CF uptake may instead depend upon active transport of the hydrolyzed 6-CF from the sinusoids, a process that our data indicate would be profoundly inhibited by rifampin.

Digital image analysis can extend intravital microscopy into a quantitative tool, but quantitative analysis of fluorescence intensity data places rigorous requirements on the methods of image collection. In order to interpret the kinetics of transport from changes in the fluorescence in a microscope image, one must ensure that fluorescence signals are collected in the linear range of the detectors, that a reliable estimate of background is measured and a level of spatial and temporal resolution obtained with sufficient signal-to-noise to capture the relevant kinetics. In order to pool data collected in different studies, consistent collection parameters must be fastidiously maintained, using the same optical components and the same detector and illumination settings (ideally verified by collecting images of fluorescent standards). Intravital microscopy incurs additional complications for quantitative analysis. Since signal levels decrease as a function of depth in living tissues, measurements must be obtained from the same depth in the organ, or measured as a quotient that corrects for the effects of depth. Capturing changes in fluorescence in sub-cellular structures requires methods of tissue immobilization that are not necessary for studies of cultured cells. Although we have developed methods of physical immobilization that provide this level of stability for studies of the liver, such stabilization is more complicated in other organs. We recently described a digital image analysis approach that we developed to correct for nonlinear motion artifacts in intravital microscopy images of the lung and other organs.<sup>59,60</sup>

While the physiology of the sample is always a concern in studies of living samples, intravital microscopy requires additional accommodations to ensure that the experimental animal is both properly sedated and physiologically supported. However, even with these precautions, local injury to the imaged tissue must be considered. For example, in our studies evidence

of minimal capsular inflammation was observed in 12/19 rats following intravital microscopy, as compared with 0/10 in rats that had not undergone microscopy. While these inflammatory responses are unlikely to affect the kinds of short-term kinetic analyses reported here, they must be considered in long-term or longitudinal studies.

Finally, one must understand the characteristics of the fluorescent probe to be used for quantitative studies. Although both sodium fluorescein and 6-CF have been validated as probes for assaying hepatic transport function, data collected with these probes must be evaluated cautiously. As noted above, our data suggest that 6-CF loading of hepatocytes may not effectively occur by free permeation of 6-CFDA *in vivo* as it does *in vitro*. In addition, the fluorescence of fluorescein is environmentally sensitive, so that the amounts of fluorescence in different compartments cannot necessarily be used as accurate indicators of the amount of probe in different compartments. Fluorescein fluorescence is quenched at low pH, and is reduced by protein binding and glucuronidation. The significance of fluorescein's pH sensitivity for evaluating hepatic transport is likely to be minimal, since its itinerary through the liver does not include particularly acidic compartments. Since the vast majority of fluorescein is bound to serum proteins following intravenous injection,<sup>48</sup> the effect of protein binding may be more significant. Thus, comparisons of fluorescence levels in different compartments must be tempered with consideration of potential differences in protein binding. Finally, because the majority of fluorescein is glucuronidated within 30 min of intravenous injection,<sup>47,48</sup> a modification that reduces fluorescein fluorescence by 85–95%,<sup>47,48</sup> long-term kinetics studies using sodium fluorescein as a probe may be difficult to interpret.

Although the factors discussed above suggest that caution must be applied to interpretations of relative fluorescence levels in different cellular compartments, one of the more surprising results of the studies presented here is that there appears to be a large disparity between the rate at which sodium fluorescein is transported into hepatocytes and the rate at which it is secreted into canaliculi. In each of the three control rats studied here, the rate at which the mean fluorescence of the cytosol increased (1562, 1263 and 1391 AU per minute) approximately equals the rate at which the mean fluorescence in canaliculi increased (1735, 841 and 1263 AU per minute). When one considers the vastly larger volume of the cytosol relative to the canaliculus, the comparable increases in the mean fluorescence of the cytosol and the canaliculus suggest that much more probe is internalized into hepatocytes than is secreted to the canaliculus. While this observation conflicts with the simple, vectorial model of hepatic transport, it is supported by recent studies suggesting that sinusoidal reflux is an important component of hepatocyte transport. Studies from the laboratory of Schinkel have associated conjugated hyperbilirubinemia with the absence of functional organic anion transport function in both mice and humans.<sup>54,61</sup> Since organic anion transporters are believed to be responsible for delivery of bilirubin to the hepatocyte cytosol, where conjugation occurs, this is a surprising result. In the model used to explain these results, the authors suggest that organic anion transporters mediate re-uptake

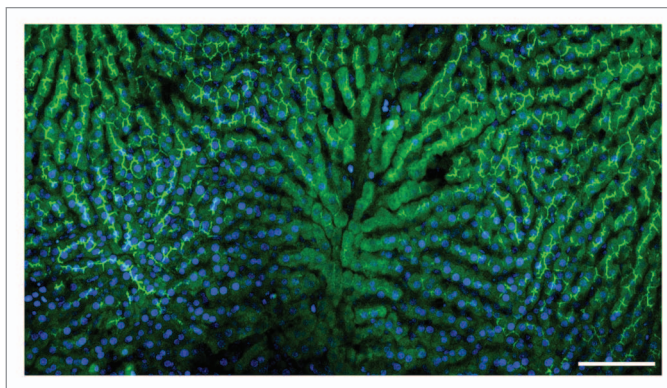


**Figure 5.** Spatial variability in sodium fluorescein transport in the rat liver. Montage projection of 3 image volumes collected from the liver of a rat 10 min after intravenous injection of sodium fluorescein. Nuclei are labeled with Hoechst 33342, introduced prior to injection of sodium fluorescein. Whereas periportal regions (left and right in the field) show dim cytosolic and bright canalicular fluorescence, pericentral hepatocytes (center of the field) are characterized by a stronger partitioning of probe to the cytosol. Scale bar represents a distance of 100 microns.

of bilirubin that is refluxed by hepatocytes after conjugation (via Mrp3 and/or Mrp4). In this model, vectorial hepatic transport is an iterative process, involving multiple rounds of uptake and secretion by different hepatocytes arrayed sequentially along the periportal-pericentral axis of the liver lobule.

Our *in vivo* data are broadly consistent with this model. In addition to suggesting a significant sinusoidal reflux of internalized probes, our studies consistently identify significant differences in transport along the periportal-pericentral axis of the liver lobule. **Figure 5** shows a montage of 3 image volumes collected from the liver of a living rat, 10 min after intravenous injection of sodium fluorescein. Using blood flow to establish the periportal and pericentral regions of the liver, we consistently observe significantly lower levels of cytosolic fluorescein in periportal hepatocytes (at left and right in the field of **Fig. 5**) than in pericentral hepatocytes (center of the field in **Fig. 5**), consistent with the notion of enhanced hepatocyte reflux in periportal hepatocytes.

In summary, we have demonstrated how intravital microscopy can be used to directly measure individual processes of hepatic transport *in vivo*, providing unique insights into the dynamics of hepatocyte transport. Results presented extend previous studies of cultured cells, demonstrating that rifampin inhibits uptake of organic anions by hepatocytes *in vivo* and provide support for an iterative model of hepatic transport. Although used here to evaluate the effects of chronic rifampin treatment, the ability to analyze processes occurring in the timescale of seconds to minutes also provides intravital microscopy with the unique ability to detect acute, or transient drug effects which, when combined with additional readouts of injury,<sup>43,60,62–66</sup> provides the potential to characterize the chronology of cholestatic liver injury. Since cholestatic drugs can induce complex changes in transport and metabolism within minutes of administration, these kinds of characterizations may be critical to understanding the causes and progression of cholestatic liver injury.

## Materials and Methods

**Preparation of the rat for intravital microscopy.** All animal studies were conducted in compliance with the Institutional Animal Care and Use Committee guidelines of Indiana University. Adult Sprague Dawley rats, weighing between 180 and 300 g, were sedated with 5% Isoflurane, weighed and 130 mg/kg Inactin was administered intraperitoneally for anesthesia. During surgery, the rat is placed on a heating pad in order to maintain the rat's body temperature. Additionally, the rat's body temperature is monitored using a rectal thermometer and the rat's heart rate is monitored visually. In order to determine that the rat is anesthetized, the rat's reflexes are evaluated through pinching of ears and feet. Once anesthetized, a 3 cm x 1.5 cm L-shaped incision is made in the neck, a jugular cannulation is placed using PE 50 tubing filled with sterile 0.9% saline and attached to a Luer stub adaptor and 1 mL syringe, and the neck is sutured with 3-0 black silk sterile suture. At this time, a bolus of Hoechst 33342 (Invitrogen, 2 mg/kg) diluted in 0.9% sterile saline to a total 0.4 mL is injected into the jugular line to label cell nuclei. To expose the liver for imaging, a 4 cm incision is made across the torso 1 to 2 cm below the middle of the rib cage. A wet (0.9% saline) 2 x 2 gauze sponge is gently placed below the left lateral liver lobe. The liver is secured for microscopy by tethering the liver to the bottom of a Willco coverslip-bottomed dish (GWST-5040), as follows. Tape is placed on the periphery of the glass window of the dish, and cyanoacrylate glue is applied to the tape. The glass is pressed to the liver and the gauze on either side of the liver is gently pressed and glued to the tape using cotton-tipped applicators. Sterile 0.9% saline is then placed in the coverslip-bottomed dish to keep liver moist throughout the imaging session. For evaluation of the effects of rifampin, animals were administered either rifampin (250 mg/kg) or vehicle (25% PEG400, 5% DMSO in purified water) by oral gavage daily for four days prior to analysis.

**Intravital microscopy.** Data presented in **Figures 1, 3 and 4** were collected using an Olympus Fluoview 1000 laser scanning confocal microscope system modified for multiphoton fluorescence excitation imaging, using an Olympus 20X, NA 0.95 objective. The system is mounted to an IX81 inverted microscope stand and is modified with the addition of a Spectraphysics MaiTai titanium sapphire laser (Spectraphysics), a Pockels cell electro-optical attenuator (Conoptics Inc.), a Keplerian collimator/beam expander and a custom designed, 3 channel external detector system equipped with gallium arsenide phosphide detectors (Hamamatsu) and 380–480 nm, 500–550 nm and 560–650 nm barrier filters. Data presented in **Figures 2 and 5** were collected using an Olympus Fluoview 1000 MPE laser scanning confocal/multiphoton microscope system, using an Olympus

25X, NA 1.05, IR optimized water immersion objective. This system is mounted to an IX81 inverted microscope stand, equipped with a Spectraphysics MaiTai DeepSee titanium sapphire laser (Spectraphysics) with a four channel external detector system using 380–480 nm, 500–550 nm and 560–650 nm barrier filters. In both cases, fluorescence was excited using 800 nm illumination and images collected at a rate of approximately one frame per second, with stacks for each time point collected at a rate between 6 and 12 per minute.

For intravital microscopy, the rat is gently placed onto the microscope stage, and the coverslip bottomed dish is taped to the stage adaptor. To keep the rat and liver at a normal body temp, zoological heating pads are placed beneath the rat, an objective heater is placed on the objective, and a heating blanket is placed over the rat. For transport studies, images are collected immediately after injection of a bolus of sodium fluorescein (SF, Sigma-Aldrich, 2.5 mg/kg) or 6-Carboxyfluorescein diacetate (6-CFDA, Sigma-Aldrich, 0.2 mg/kg) diluted in 0.9% sterile saline to a total 0.4 mL, injected via the jugular cannulation.

**Data analysis and presentation.** Quantitative image analysis was conducted using Metamorph image processing software (Molecular Devices). Quantitative analysis was conducted on raw image data, but images presented in **Figures** were both contrast enhanced (re-setting minimum and maximal values, and adjusting gamma to 0.85) and smoothed, using a Gaussian filter. In color images, the visibility of Hoechst-labeled nuclei was enhanced by selectively adjusting the hue, saturation and lightness of the blue channel. In all cases, images to be compared were processed identically and in such a way that the processing preserved the visibility of both the dim and bright structures of the original image. Images were processed, assembled into figures and annotated using Adobe Photoshop (Adobe). Graphics were produced and summary statistics obtained using Kaleidagraph (Synergy Software).

### Disclosure of Potential Conflicts of Interest

No potential conflicts of interest were disclosed.

### Acknowledgments

The authors wish to thank Laura Boone (Covance, Inc.) and Naga Chalansani (Indiana University) for helpful discussions and insights. These studies were partially supported by funds from the National Institutes of Health (NIH-NIAID T32 AI060519 (J. Ryan) and were conducted at the Indiana Center for Biological Microscopy.

### Supplemental Material

Supplemental materials may be found here:  
[www.landesbioscience.com/journals/intravital/article/21296](http://www.landesbioscience.com/journals/intravital/article/21296)

## References

- Temple RJ, Himmel MH. Safety of newly approved drugs: implications for prescribing. *JAMA* 2002; 287:2273-5; PMID:11980528; <http://dx.doi.org/10.1001/jama.287.17.2273>.
- Lee WM. Drug-induced hepatotoxicity. *N Engl J Med* 2003; 349:474-85; PMID:12890847; <http://dx.doi.org/10.1056/NEJMra021844>.
- Roma MG, Crocenzi FA, Mottino AD. Dynamic localization of hepatocellular transporters in health and disease. *World J Gastroenterol* 2008; 14:6786-801; PMID:19058304; <http://dx.doi.org/10.3748/wjg.14.6786>.
- Crocenzi FA, Zucchetti AE, Boaglio AC, Barosso IR, Sanchez Pozzi EJ, Mottino AD, et al. Localization status of hepatocellular transporters in cholestasis. *Frontiers in bioscience: a journal and virtual library* 2012; 17:1201-18.
- Zollner G, Wagner M, Trauner M. Nuclear receptors as drug targets in cholestasis and drug-induced hepatotoxicity. *Pharmacol Ther* 2010; 126:228-43; PMID:20388526; <http://dx.doi.org/10.1016/j.pharmthera.2010.03.005>.
- Wagner M, Zollner G, Trauner M. Nuclear receptor regulation of the adaptive response of bile acid transporters in cholestasis. *Semin Liver Dis* 2010; 30:160-77; PMID:20422498; <http://dx.doi.org/10.1055/s-0030-1253225>.
- Mottino AD, Catania VA. Hepatic drug transporters and nuclear receptors: regulation by therapeutic agents. *World J Gastroenterol* 2008; 14:7068-74; PMID:19084913; <http://dx.doi.org/10.3748/wjg.14.7068>.
- Donner MG, Keppler D. Up-regulation of basolateral multidrug resistance protein 3 (Mrp3) in cholestatic rat liver. *Hepatology* 2001; 34:351-9; PMID:11481620; <http://dx.doi.org/10.1053/jhep.2001.26213>.
- Paulusma CC, Kothe MJ, Bakker CT, Bosma PJ, van Bokhoven I, van Marle J, et al. Zonal down-regulation and redistribution of the multidrug resistance protein 2 during bile duct ligation in rat liver. *Hepatology* 2000; 31:684-93; PMID:10706559; <http://dx.doi.org/10.1002/hep.510310319>.
- Donner MG, Warskulat U, Saha N, Häussinger D. Enhanced expression of basolateral multidrug resistance protein isoforms Mrp3 and Mrp5 in rat liver by LPS. *Biol Chem* 2004; 385:331-9; PMID:15134348; <http://dx.doi.org/10.1515/BC.2004.029>.
- Theruvath TP, Zhong Z, Currin RT, Ramshesh VK, Lemasters JJ. Endothelial nitric oxide synthase protects transplanted mouse livers against storage/reperfusion injury: Role of vasodilatory and innate immunity pathways. *Transplant Proc* 2006; 38:3351-7; PMID:17175270; <http://dx.doi.org/10.1016/j.transproceed.2006.10.171>.
- Mathes AM, Kubulus D, Pradarutti S, Bentley A, Weiler J, Wolf B, et al. Melatonin pretreatment improves liver function and hepatic perfusion after hemorrhagic shock. *Shock* 2008; 29:112-8; PMID:17666950.
- Furrer K, Tian Y, Pfammatter T, Jochum W, El-Badry AM, Graf R, et al. Selective portal vein embolization and ligation trigger different regenerative responses in the rat liver. *Hepatology* 2008; 47:1615-23; PMID:18395841; <http://dx.doi.org/10.1002/hep.22164>.
- Rehman H, Connor HD, Ramshesh VK, Theruvath TP, Mason RP, Wright GL, et al. Ischemic preconditioning prevents free radical production and mitochondrial depolarization in small-for-size rat liver grafts. *Transplantation* 2008; 85:1322-31; PMID:18475191; <http://dx.doi.org/10.1097/TP.0b013e31816de302>.
- Theruvath TP, Zhong Z, Pedititakis P, Ramshesh VK, Currin RT, Tikonov A, et al. Minocycline and N-methyl-4-isoleucine cyclosporin (NIM811) mitigate storage/reperfusion injury after rat liver transplantation through suppression of the mitochondrial permeability transition. *Hepatology* 2008; 47:236-46; PMID:18023036; <http://dx.doi.org/10.1002/hep.21912>.
- Zhong Z, Theruvath TP, Currin RT, Waldmeier PC, Lemasters JJ. NIM811, a mitochondrial permeability transition inhibitor, prevents mitochondrial depolarization in small-for-size rat liver grafts. *Am J Transplant* 2007; 7:1103-11; PMID:17456198; <http://dx.doi.org/10.1111/j.1600-6143.2007.01770.x>.
- Rehman H, Sun J, Shi Y, Ramshesh VK, Liu Q, Currin RT, et al. NIM811 prevents mitochondrial dysfunction, attenuates liver injury, and stimulates liver regeneration after massive hepatectomy. *Transplantation* 2011; 91:406-12; PMID:21131897.
- Rehman H, Ramshesh VK, Theruvath TP, Kim I, Currin RT, Giri S, et al. NIM811 (N-methyl-4-isoleucine cyclosporine), a mitochondrial permeability transition inhibitor, attenuates cholestatic liver injury but not fibrosis in mice. *J Pharmacol Exp Ther* 2008; 327:699-706; PMID:18801946; <http://dx.doi.org/10.1124/jpet.108.143578>.
- Zhong Z, Ramshesh VK, Rehman H, Currin RT, Sridharan V, Theruvath TP, et al. Activation of the oxygen-sensing signal cascade prevents mitochondrial injury after mouse liver ischemia-reperfusion. *Am J Physiol Gastrointest Liver Physiol* 2008; 295:G823-32; PMID:18772364; <http://dx.doi.org/10.1152/ajpgi.90287.2008>.
- Li FC, Huang GT, Lin CJ, Wang SS, Sun TL, Lo SY, et al. Apical membrane rupture and backward bile flooding in acetaminophen-induced hepatocyte necrosis. *Cell death & disease* 2011; 2:e183.
- Goetz M, Ansems JV, Galle PR, Schuchmann M, Kiesslich R. *In vivo* real-time imaging of the liver with confocal endomicroscopy permits visualization of the temporospatial patterns of hepatocyte apoptosis. *Am J Physiol Gastrointest Liver Physiol* 2011; 301:G764-72; PMID:21778462; <http://dx.doi.org/10.1152/ajpgi.00175.2011>.
- Khandoga A, Kessler JS, Hanschen M, Khandoga AG, Burggraf D, Reichel C, et al. Matrix metalloproteinase-9 promotes neutrophil and T cell recruitment and migration in the postschemic liver. *J Leukoc Biol* 2006; 79:1295-305; PMID:16551680; <http://dx.doi.org/10.1189/jlb.0805468>.
- McDonald B, McAvoy EF, Lam F, Gill V, de la Motte C, Savani RC, et al. Interaction of CD44 and hyaluronan is the dominant mechanism for neutrophil sequestration in inflamed liver sinusoids. *J Exp Med* 2008; 205:915-27; PMID:18362172; <http://dx.doi.org/10.1084/jem.20071765>.
- McDonald B, Pittman K, Menezes GB, Hirota SA, Slaba I, Waterhouse CC, et al. Intravascular danger signals guide neutrophils to sites of sterile inflammation. *Science* 2010; 330:362-6; PMID:20947763; <http://dx.doi.org/10.1126/science.1195491>.
- Oda M, Han JY, Nakamura M. Endothelial cell dysfunction in microvasculature: relevance to disease processes. *Clin Hemorheol Microcirc* 2000; 23:199-211; PMID:11321441.
- Foitzik T, Eibl G, Hotz B, Hotz H, Kahrau S, Kasten C, et al. Persistent multiple organ microcirculatory disorders in severe acute pancreatitis: experimental findings and clinical implications. *Dig Dis Sci* 2002; 47:130-8; PMID:11837713; <http://dx.doi.org/10.1023/A:1013284008219>.
- Lendemans S, Peszko A, Oberbeck R, Schmitz D, Husain B, Burkhard M, et al. Microcirculatory alterations of hepatic and mesenteric microcirculation in endotoxin tolerance. *Shock* 2008; 29:223-31; PMID:18386390.
- Keller SA, Paxian A, Ashburn JH, Clemens MG, Huynh T. Kupffer cell ablation improves hepatic microcirculation after trauma and sepsis. *J Trauma* 2005; 58:740-9, discussion 749-51; PMID:15824650; <http://dx.doi.org/10.1097/01.TA.0000158246.74816.18>.
- Theruvath TP, Snoddy MC, Zhong Z, Lemasters JJ. Mitochondrial permeability transition in liver ischemia and reperfusion: role of c-Jun N-terminal kinase 2. *Transplantation* 2008; 85:1500-4; PMID:18497693; <http://dx.doi.org/10.1097/TP.0b013e31816febf5>.
- Sun CK, Zhang XY, Zimmermann A, Davis G, Wheatley AM. Effect of ischemia-reperfusion injury on the microcirculation of the steatotic liver of the Zucker rat. *Transplantation* 2001; 72:1625-31; PMID:11726821; <http://dx.doi.org/10.1097/00007890-200111270-00008>.
- Farrell GC, Teoh NC, McCuskey RS. Hepatic microcirculation in fatty liver disease. *Anat Rec (Hoboken)* 2008; 291:684-92; PMID:18484615; <http://dx.doi.org/10.1002/ar.20715>.
- Tanaka K, Morimoto Y, Toiyama Y, Matsushita K, Kawamura M, Koike Y, et al. In vivo time-course imaging of tumor angiogenesis in colorectal liver metastases in the same living mice using two-photon laser scanning microscopy. *Journal of oncology* 2012; 2012:265487.
- Lee HS, Liu Y, Chen HC, Chiou LL, Huang GT, Lo W, et al. Optical biopsy of liver fibrosis by use of multiphoton microscopy. *Opt Lett* 2004; 29:2614-6; PMID:15526622; <http://dx.doi.org/10.1364/OL.29.002614>.
- Hanson V. Liver cell secretion under normal and pathologic conditions studied by fluorescence microscopy on living rats. *Acta Physiol Scand Suppl* 1952; 28:1-268; PMID:13007504.
- Bhathal PS, Christie GS. Intravital fluorescence microscopy of the terminal and subterminal portions of the biliary tree of normal guinea pigs and rats. *Lab Invest* 1969; 20:472-9; PMID:5767419.
- Holzinger F, Krähenbühl L, Scheingart CD, Ton-Nu HT, Hofmann AF. Use of a fluorescent bile acid to enhance visualization of the biliary tract and bile leaks during laparoscopic surgery in rabbits. *Surg Endosc* 2001; 15:209-12; PMID:11285970; <http://dx.doi.org/10.1007/s004640000265>.
- Liu Y, Chen HC, Yang SM, Sun TL, Lo W, Chiou LL, et al. Visualization of hepatobiliary excretory function by intravital multiphoton microscopy. *J Biomed Opt* 2007; 12:014014; PMID:17343489; <http://dx.doi.org/10.1117/1.2710237>.
- Li FC, Liu Y, Huang GT, Chiou LL, Liang JH, Sun TL, et al. *In vivo* dynamic metabolic imaging of obstructive cholestasis in mice. *Am J Physiol Gastrointest Liver Physiol* 2009; 296:G1091-7; PMID:19246634; <http://dx.doi.org/10.1152/ajpgi.90681.2008>.
- Sherman IA, Fisher MM. Hepatic transport of fluorescent molecules: *in vivo* studies using intravital TV microscopy. *Hepatology* 1986; 6:444-9; PMID:3710433; <http://dx.doi.org/10.1002/hep.1800603021>.
- Roberts MS, Roberts MJ, Robertson TA, Sanchez W, Thorling C, Zou Y, et al. In vitro and in vivo imaging of xenobiotic transport in human skin and in the rat liver. *Journal of biophotonics* 2008; 1:478-93.
- Thorling CA, Dancik Y, Hupple CW, Medley G, Liu X, Zvyagin AV, et al. Multiphoton microscopy and fluorescence lifetime imaging provide a novel method in studying drug distribution and metabolism in the rat liver *in vivo*. *J Biomed Opt* 2011; 16:086013; PMID:21895325; <http://dx.doi.org/10.1117/1.3614473>.
- Watanabe N, Tsukada N, Smith CR, Phillips MJ. Motility of bile canaliculi in the living animal: implications for bile flow. *J Cell Biol* 1991; 113:1069-80; PMID:2040644; <http://dx.doi.org/10.1083/jcb.113.5.1069>.

43. Dunn KW, Sandoval RM, Kelly KJ, Dagher PC, Tanner GA, Atkinson SJ, et al. Functional studies of the kidney of living animals using multicolor two-photon microscopy. *Am J Physiol Cell Physiol* 2002; 283:C905-16; PMID:12176747.
44. Barth CA, Schwarz LR. Transcellular transport of fluorescein in hepatocyte monolayers: evidence for functional polarity of cells in culture. *Proc Natl Acad Sci U S A* 1982; 79:4985-7; PMID:6956908; <http://dx.doi.org/10.1073/pnas.79.16.4985>.
45. Gebhardt R, Jung W. Biliary secretion of sodium fluorescein in primary monolayer cultures of adult rat hepatocytes and its stimulation by nicotinamide. *J Cell Sci* 1982; 56:233-44; PMID:6220021.
46. De Bruyn T, Fattah S, Stieger B, Augustijns P, Annaert P. Sodium fluorescein is a probe substrate for hepatic drug transport mediated by OATP1B1 and OATP1B3. *J Pharm Sci* 2011; 100:5018-30; PMID:21837650; <http://dx.doi.org/10.1002/jps.22694>.
47. Blair NP, Evans MA, Lesar TS, Zeimer RC. Fluorescein and fluorescein glucuronide pharmacokinetics after intravenous injection. *Invest Ophthalmol Vis Sci* 1986; 27:1107-14; PMID:3721789.
48. Chahal PS, Neal MJ, Kohner EM. Metabolism of fluorescein after intravenous administration. *Invest Ophthalmol Vis Sci* 1985; 26:764-8; PMID:3997424.
49. Webb JM, Fonda M, Brouwer EA. Metabolism and excretion patterns of fluorescein and certain halogenated fluorescein dyes in rats. *J Pharmacol Exp Ther* 1962; 137:141-7; PMID:14005410.
50. Vavricka SR, Van Montfort J, Ha HR, Meier PJ, Fattinger K. Interactions of rifamycin SV and rifampicin with organic anion uptake systems of human liver. *Hepatology* 2002; 36:164-72; PMID:12085361; <http://dx.doi.org/10.1053/jhep.2002.34133>.
51. Fattinger K, Cattori V, Hagenbuch B, Meier PJ, Stieger B. Rifamycin SV and rifampicin exhibit differential inhibition of the hepatic rat organic anion transporting polypeptides, Oatp1 and Oatp2. *Hepatology* 2000; 32:82-6; PMID:10869292; <http://dx.doi.org/10.1053/jhep.2000.8539>.
52. Campbell SD, de Morais SM, Xu JJ. Inhibition of human organic anion transporting polypeptide OATP 1B1 as a mechanism of drug-induced hyperbilirubinemia. *Chem Biol Interact* 2004; 150:179-87; PMID:15535988; <http://dx.doi.org/10.1016/j.cbi.2004.08.008>.
53. Lau YY, Okochi H, Huang Y, Benet LZ. Pharmacokinetics of atorvastatin and its hydroxy metabolites in rats and the effects of concomitant rifampicin single doses: relevance of first-pass effect from hepatic uptake transporters, and intestinal and hepatic metabolism. *Drug Metab Dispos* 2006; 34:1175-81; PMID:16624870; <http://dx.doi.org/10.1124/dmd.105.009076>.
54. van de Steeg E, Wagenaar E, van der Kruijssen CM, Burggraaf JE, de Waart DR, Elferink RP, et al. Organic anion transporting polypeptide 1a/1b-knockout mice provide insights into hepatic handling of bilirubin, bile acids, and drugs. *J Clin Invest* 2010; 120:2942-52; PMID:20644253; <http://dx.doi.org/10.1172/JCI42168>.
55. Lengyel G, Veres Z, Tugyi R, Vereczkey L, Molnár T, Glavinas H, et al. Modulation of sinusoidal and canalicular elimination of bilirubin-glucuronides by rifampicin and other cholestatic drugs in a sandwich culture of rat hepatocytes. *Hepatol Res* 2008; 38:300-9; PMID:17760873; <http://dx.doi.org/10.1111/j.1872-034X.2007.00255.x>.
56. Nakanishi T, Shibue Y, Fukuyama Y, Yoshida K, Fukuda H, Shirasaka Y, et al. Quantitative time-lapse imaging-based analysis of drug-drug interaction mediated by hepatobiliary transporter, multidrug resistance-associated protein 2, in sandwich-cultured rat hepatocytes. *Drug Metab Dispos* 2011; 39:984-91; PMID:21415249; <http://dx.doi.org/10.1124/dmd.111.038059>.
57. Zamek-Gliszczyński MJ, Xiong H, Patel NJ, Turncliff RZ, Pollack GM, Brouwer KL. Pharmacokinetics of 5 (and 6)-carboxy-2',7'-dichlorofluorescein and its diacetate promoiety in the liver. *J Pharmacol Exp Ther* 2003; 304:801-9; PMID:12538836; <http://dx.doi.org/10.1124/jpet.102.044107>.
58. Cui Y, König J, Keppler D. Vectorial transport by double-transfected cells expressing the human uptake transporter SLC21A8 and the apical export pump ABCB2. *Mol Pharmacol* 2001; 60:934-43; PMID:11641421.
59. Lorenz KS, Salama P, Dunn KW, Delp EJ. Digital correction of motion artefacts in microscopy image sequences collected from living animals using rigid and nonrigid registration. *J Microsc* 2012; 245:148-60; PMID:22092443; <http://dx.doi.org/10.1111/j.1365-2818.2011.03557.x>.
60. Presson RG Jr., Brown MB, Fisher AJ, Sandoval RM, Dunn KW, Lorenz KS, et al. Two-photon imaging within the murine thorax without respiratory and cardiac motion artifact. *Am J Pathol* 2011; 179:75-82; PMID:21703395; <http://dx.doi.org/10.1016/j.ajpath.2011.03.048>.
61. van de Steeg E, Stránecký V, Hartmannová H, Nosková L, Hrbek M, Wagenaar E, et al. Complete OATP1B1 and OATP1B3 deficiency causes human Rotor syndrome by interrupting conjugated bilirubin reuptake into the liver. *J Clin Invest* 2012; 122:519-28; PMID:22232210; <http://dx.doi.org/10.1172/JCI59526>.
62. Babbey CM, Ahktar N, Wang E, Chen CC, Grant BD, Dunn KW. Rab10 regulates membrane transport through early endosomes of polarized Madin-Darby canine kidney cells. *Mol Biol Cell* 2006; 17:3156-75; PMID:16641372; <http://dx.doi.org/10.1091/mbc.E05-08-0799>.
63. Dunn KW, Sandoval RM, Molitoris BA. Intravital imaging of the kidney using multiparameter multiphoton microscopy. *Nephron Exp Nephrol* 2003; 94:e7-11; PMID:12806182; <http://dx.doi.org/10.1159/000070813>.
64. Dunn KW, Sutton TA, Sandoval RM. Live-animal imaging of renal function by multiphoton microscopy. *Curr Protoc Cytom* 2007; Chapter 12:Unit12.9.
65. Kalakeche R, Hato T, Rhodes G, Dunn KW, El-Achkar TM, Plotkin Z, et al. Endotoxin uptake by S1 proximal tubular segment causes oxidative stress in the downstream S2 segment. *J Am Soc Nephrol* 2011; 22:1505-16; PMID:21784899; <http://dx.doi.org/10.1681/ASN.2011020203>.
66. Kelly KJ, Sandoval RM, Dunn KW, Molitoris BA, Dagher PC. A novel method to determine specificity and sensitivity of the TUNEL reaction in the quantitation of apoptosis. *Am J Physiol Cell Physiol* 2003; 284:C1309-18; PMID:12676658.